

JPL Publication 91-9

IN-48-0R

55-146

P-39

A Pacific Ocean General Circulation Model for Satellite Data Assimilation

Y. Chao
University of California
Los Angeles

D. Halpern
Jet Propulsion Laboratory

C. R. Mechoso
University of California
Los Angeles

February 1991

NASA

National Aeronautics and
Space Administration

Jet Propulsion Laboratory
California Institute of Technology
Pasadena, California

(NASA-CR-109447) A PACIFIC OCEAN GENERAL
CIRCULATION MODEL FOR SATELLITE DATA
ASSIMILATION (JPL) 39 p CSCL 0&C

N92-12384

Unclass
G3/48 0052246



JPL Publication 91-9

A Pacific Ocean General Circulation Model for Satellite Data Assimilation

Y. Chao
University of California
Los Angeles

D. Halpern
Jet Propulsion Laboratory

C. R. Mechoso
University of California
Los Angeles

February 1991

NASA

National Aeronautics and
Space Administration

Jet Propulsion Laboratory
California Institute of Technology
Pasadena, California

The research described in this publication was carried out, in part, by the Jet Propulsion Laboratory, California Institute of Technology, under a contract with the National Aeronautics and Space Administration.

Reference herein to any specific commercial product, process, or service by trade name, trademark, manufacturer, or otherwise, does not constitute or imply its endorsement by the United States Government or the Jet Propulsion Laboratory, California Institute of Technology.

Abstract

A tropical Pacific Ocean General Circulation Model (OGCM) to be used in satellite data assimilation studies is described. The transfer of the OGCM from a CYBER-205 at NOAA's Geophysical Fluid Dynamics Laboratory to a CRAY-2 at NASA's Ames Research Center is documented. Two 3-year model integrations from identical initial conditions but performed on those two computers are compared. The model simulations are very similar to each other, as expected, but the simulation performed with the higher-precision CRAY-2 is smoother than that with the lower-precision CYBER-205. The CYBER-205 and CRAY-2 use 32 and 64-bit mantissa arithmetic, respectively.

The major features of the oceanic circulation in the tropical Pacific, namely the North Equatorial Current, the North Equatorial Countercurrent, the South Equatorial Current, and the Equatorial Undercurrent, are realistically produced and their seasonal cycles are described. The OGCM provides a powerful tool for study of tropical oceans and for assimilation of satellite altimetry data.

Acknowledgements

We are grateful to S. George H. Philander (Princeton University) and William J. Hurlin (GFDL) for their extensive encouragement and help. This work is supported by NASA RTOP No. 578-21-13 to JPL and by JPL Contract No. 958658 to UCLA. Computations were performed at NASA's Ames Research Center Numerical Aerodynamics Simulation facility.

Contents

Abstract.....	iii
Acknowledgements.....	iv
1 Introduction.....	1
2 Description of the Ocean General Circulation Model.....	1
2.1 Governing equations.....	2
2.2 Subgrid-scale parameterizations.....	3
2.3 Boundary conditions.....	5
2.4 Model design.....	6
3 Comparison of model simulations on CRAY-2 and CYBER-205.....	6
4 Climatological seasonal cycle.....	7
5 Discussion.....	8
References.....	9

~~SECRET~~ INTENTIONALLY ~~CLASSIFIED~~

1 Introduction

Over the next decade, many initiatives in remote sensing of the ocean are planned. The European Space Agency ERS-1 satellite will be launched in May 1991. The TOPEX/POSEIDON altimeter mission is scheduled for launch in the middle of 1992, and more altimeter missions are planned in the NASA Earth Observing System (EOS) program. These altimeter missions will provide precise and accurate measurements of sea surface height for many years.

Satellite altimeter data, however, only measure information on the ocean surface. Techniques have to be developed to extrapolate surface information throughout the ocean interior. This is achieved by assimilating satellite measurements into Ocean General Circulation Models (OGCMs). The objective of the data assimilation is to obtain dynamically consistent, three-dimensional distributions of oceanographic variables throughout the ocean. The resulting synoptic description of the ocean is essential for the understanding of ocean circulation and the assessment of global climate change.

Oceanic data assimilation is still in its developing stage and there are few analyses of OGCM simulations combined with assimilation of data (Ghil and Malanotte-Rizzoli, 1991). Techniques for oceanic data assimilation are mostly confined to simple oceanographic models (e.g., shallow-water model or quasi-geostrophic model), which do not adequately describe the flow and thermal fields in tropical oceans. Preliminary assimilation experiments of oceanic *in situ* measurements with OGCMs have been started in the Pacific (Derber and Rosati, 1989; Leetmaa and Ji, 1989) and in the Atlantic (Morlière *et al.*, 1989; Carton and Hackert, 1989).

Satellite data assimilation is currently under way in a joint project at the Jet Propulsion Laboratory and University of California, Los Angeles. The project addresses a major question: to what extent can the assimilation of satellite sea surface height measurements improve the simulation of oceanic circulation by OGCMs?

The purpose of this report is twofold: (1) to give a brief description of the OGCM, and (2) to document the transfer of the OGCM from a CYBER-205 at NOAA's Geophysical Fluid Dynamics Laboratory (GFDL) to a CRAY-2 at NASA's Ames Research Center.

2 Description of the Ocean General Circulation Model

The GFDL OGCM was selected for satellite data assimilation because it can produce realistic simulations of current and temperature distributions in the tropical oceans. Over the past twenty years, the GFDL OGCM has undergone continuous improvement and is currently widely used in the U.S., Europe and Japan. A modified version of the GFDL OGCM (Philander *et al.*, 1987) played a very important role in recent developments of dynamic oceanography in tropical oceans. This OGCM was first to produce a successful simulation of the El Niño Southern Oscillation phenomenon (Philander and Seigel, 1985; Philander *et al.*,

1990). A version of this model is operationally run at NOAA's National Meteorological Center (NMC); the model output is published each month in the *Climate Diagnostic Bulletin*, which provides a continuing description of monthly oceanographic conditions in the tropical Pacific. The GFDL OGCM, in one form or another, is expected to play a central role in the Tropical Ocean and Global Atmosphere (TOGA), World Ocean Circulation Experiment (WOCE), and EOS programs.

2.1 Governing equations

Developments of GFDL OGCM started more than two decades ago. Since then, the model has been used to study some of the most basic aspects of large scale, baroclinic oceanic circulation. A description of the model physics and numerical methods was published by Bryan (1969), and the model code was described by Cox (1984). The model is based on the primitive equations with the Boussinesq and hydrostatic approximations. The model's prognostic variables are the zonal velocity component (u), meridional velocity component (v), temperature (T), and salinity (S). The model's diagnostic variables are vertical velocity component (w), pressure (P) and density (ρ). The governing equations of the model are

$$\frac{\partial u}{\partial t} + \Gamma(u) - \left(\frac{u \tan \phi}{a} + 2\Omega n \right) v = -ma^{-1}\rho^{-1} \frac{\partial P}{\partial \lambda} + \frac{\partial}{\partial z} (\overline{-w'u'}) + F_\lambda, \quad (1a)$$

$$\frac{\partial v}{\partial t} + \Gamma(v) + \left(\frac{u \tan \phi}{a} + 2\Omega n \right) u = -a^{-1}\rho^{-1} \frac{\partial P}{\partial \phi} + \frac{\partial}{\partial z} (\overline{-w'v'}) + F_\phi, \quad (1b)$$

$$\frac{\partial T}{\partial t} + \Gamma(T) = \frac{\partial}{\partial z} (\overline{-w'T'}) + F_T, \quad (1c)$$

$$\frac{\partial S}{\partial t} + \Gamma(S) = \frac{\partial}{\partial z} (\overline{-w'S'}) + F_S, \quad (1d)$$

$$\Gamma(1) = 0, \quad (1e)$$

$$\frac{\partial P}{\partial z} = -\rho g, \quad (1f)$$

$$\rho = \rho(T, S, z), \quad (1g)$$

where λ is longitude, ϕ is latitude, z is depth, a is radius of the earth, g is gravitational acceleration, Ω is angular velocity of the earth, $m = \sec \phi$, and $n = \sin \phi$. The coordinate directions λ , ϕ and z are towards east, north and upward, respectively. The three-dimensional advection operator is defined as

$$\Gamma(\mu) = ma^{-1} \frac{\partial}{\partial \lambda} (u\mu) + a^{-1} \frac{\partial}{\partial \phi} (v\mu) + \frac{\partial}{\partial z} (w\mu), \quad (2)$$

where μ represents u , v , T or S . The horizontal friction terms are

$$F_\lambda = A_{MH} \left[\nabla^2 u + a^{-2} (1 - \tan^2 \phi) u - 2m^2 n a^{-2} \frac{\partial v}{\partial \lambda} \right], \quad (3a)$$

$$F_\phi = A_{MH} \left[\nabla^2 v + a^{-2} (1 - \tan^2 \phi) v - 2m^2 n a^{-2} \frac{\partial u}{\partial \lambda} \right], \quad (3b)$$

$$F_T = A_{TH} \nabla^2 T, \quad (3c)$$

$$F_S = A_{TH} \nabla^2 S, \quad (3d)$$

where A_{MH} and A_{TH} are the coefficients of horizontal eddy viscosity and diffusivity, and

$$\nabla^2 \mu = m^2 a^{-2} \frac{\partial^2 \mu}{\partial \lambda^2} + m a^{-2} \frac{\partial}{\partial \phi} \left(m^{-1} \frac{\partial \mu}{\partial \phi} \right). \quad (4)$$

The equation of state is expressed by an empirical polynomial fit to the Knudsen formula described in Bryan and Cox (1972).

2.2 Subgrid-scale parameterizations

In the governing equations (1a) - (1g), the u , v , w , T , and S represent ensemble mean variables, which are resolved on the model grid, the primes represent subgrid-scale turbulence fields, and overbars represent ensemble means of subgrid-scale turbulence fluxes. In order to solve the governing equations, turbulent fluxes, i.e., $\overline{w'u'}$, $\overline{w'v'}$, $\overline{w'T'}$, and $\overline{w'S'}$, have to be parameterized. The first-order turbulence closure scheme assumes that

$$\overline{w'A'} = -K_z \frac{\partial A}{\partial z}, \quad (5)$$

where A represents u , v , T or S , and K_z is the vertical eddy exchange coefficient. In the early version of the GFDL OGCM (Bryan 1969; Cox 1984), K_z was assumed to be a constant. This scheme of constant vertical mixing has problems when it is applied to tropical oceans, because the model-simulated ocean is highly sensitive to the K_z value (Philander and Pacanowski, 1980; Semtner and Holland, 1980). For example, although the vertical resolutions in these two models are comparable (16 levels in Philander and Pacanowski model and 14 levels in Semtner and Holland model), the Equatorial Undercurrent core speed simulated by the constant vertical mixing model varies from 0.5 m s^{-1} in an OGCM with $K_z = 1.0 \times 10^{-3} \text{ m}^2 \text{ s}^{-1}$ (Philander and Pacanowski, 1980) to 1.0 m s^{-1} in an OGCM with $K_z = 1.5 \times 10^{-4} \text{ m}^2 \text{ s}^{-1}$ (Semtner and Holland, 1980). The observed core speed of the Equatorial Undercurrent is about 1.0 cm s^{-1} according to Halpern (1987). The main reason for the Equatorial Undercurrent simulated in Semtner and Holland model to attain the core speed of 1.0 m s^{-1} is the small vertical eddy viscosity.

Measurements suggested that the vertical eddy viscosity varies considerably in the tropical oceans (Halpern, 1980). Given these considerations, a more realistic formulation of the first-order turbulence closure scheme should assume that K_z depends upon the Richardson number, Ri , which takes into account the vertical gradient of temperature and vertical shears of currents. The Richardson number is defined as

$$Ri = \frac{\beta g \left(\frac{\partial T}{\partial z} \right)}{\left(\frac{\partial u}{\partial z} \right)^2 + \left(\frac{\partial v}{\partial z} \right)^2}, \quad (6)$$

where β is the coefficient of the thermal expansion of water and is given as

$$\beta = 8.75 \times 10^{-6} (T + 9), \quad (7)$$

and T is the temperature in degrees Celsius ($^{\circ}C$). Pacanowski and Philander (1981) formulated the vertical mixing coefficient as an empirical function of Richardson number, given as

$$K_z = K_o + \frac{\gamma_o}{(1 + \alpha Ri)^n}, \quad (8)$$

where $K_o = 1.34 \times 10^{-6} \text{ m}^2 \text{ s}^{-1}$, $\gamma_o = 5.0 \times 10^{-3} \text{ m}^2 \text{ s}^{-1}$, $\alpha = 5$, and $n = 2$. Given this formulation, Philander *et al.* (1987) showed that tropical oceans can be simulated with a realistic Equatorial Undercurrent of 1.0 m s^{-1} core speed.

Parameterizations of the constant vertical mixing and Richardson number dependent mixing both belong to the first-order turbulence closure scheme. Whatever the empirical formula of Richardson number is chosen, the turbulence fluxes are always assumed to be locally related to the mean gradient described on the model grid. The subgrid-scale turbulence fields, such as the diffusion of turbulence kinetic energy, are neglected.

Rosati and Miyakoda (1988) have adapted a second-order turbulence closure scheme for the GFDL OGCM. This scheme, which corresponds to the level 2.5 turbulence closure scheme developed by Mellor and Yamada (1973, 1982), includes the turbulence kinetic energy as a prognostic variable. Model results with this second-order turbulence closure scheme showed a better simulation of the mixed layer in tropical oceans. However, the model simulation showed an Equatorial Undercurrent about 50% weaker than that observed. This deficiency could be partly due to the vertical resolution in the Rosati and Miyakoda (1988) model, where there are only 9 levels in the upper 317 m compared to 18 levels in the Philander

et al. (1987) model. Comparison studies of the second-order turbulence closure scheme and Richardson number dependent mixing are currently under way (C.-C. Ma, personal communication, 1990).

2.3 Boundary conditions

At lateral walls, a no-slip condition is applied. No flux of heat and salt is allowed on the east and west boundaries. Poleward of 20.15°S and 32.26°N, the temperature and salinity are relaxed to the climatological seasonal values (Levitus, 1982). In these regions, the temperature and salinity equations, (1c) and (1d), include an extra term of $\varepsilon(\mu - \mu^*)$, where μ^* is the climatological value and ε is a Newtonian damping coefficient. The values of ε depend upon latitude and are given in Table 1. This treatment mitigates the effect of artificial zonal walls along the southern and northern boundaries.

At the surface, a rigid lid approximation is made where vertical velocity is zero. The rigid lid assumption filters out high speed external gravity waves. The wind stress acts as a body force to the first layer of the model. The heat flux (HF) across the air-sea interface is given as

$$HF = SW - LW - QS - QL, \quad (9)$$

where SW is short wave radiative heat flux, LW is long wave radiative heat flux, QS is sensible heat flux, and QL is latent heat flux. The short wave incoming insolation SW is taken to be 242 W m⁻¹ equatorward of 20° latitude, and to decrease linearly to 145 W m⁻¹ between 20° and 45° latitude. The outgoing long wave radiation LW has a constant value of 56 W m⁻¹. The sensible and latent heat fluxes are calculated using the model-simulated sea surface temperature and the prescribed surface air temperature.

$$QS = \rho_a C_D C_P |\vec{v}| (T_o - T_a) \quad (10)$$

and

$$QL = \rho C_D L |\vec{v}| [E_o - \gamma E_a] (0.622 / 1013.25), \quad (11)$$

where ρ_a is density of air, C_D is the drag coefficient and equal to 0.0012, $|\vec{v}|$ is surface wind speed, C_P is heat capacity, T_o is sea surface temperature (°C), T_a is surface air temperature (°C), L is the latent heat of evaporation and equal to 2.5×10^6 J kg⁻¹, and the mixing ratio γ is fixed as 0.8. The saturation vapor pressure, E , is

$$E_o = 10^{9.4 - 2353/T_o}, \quad (12)$$

$$E_a = 10^{9.4 - 2353/T_a} \quad (13)$$

2.4 Model design

The governing equations, along with their boundary equations, are solved numerically by finite difference techniques with a staggered "B" grid configuration (Arakawa, 1966), as shown in Fig. 1. The time differencing is centered. The model domain covers the Pacific Ocean from 30°S to 50°N with realistic coastal geometry, as shown in Fig. 2. The longitudinal resolution of the model is 1° longitude. The latitudinal resolution is 1/3° latitude within the equatorial band of 10°S and 10°N and increases gradually to 2.5° latitude at 30°S and 50°N. The model ocean has constant depth of 4149 m. There are 27 levels in the vertical with 18 levels in the upper 317 m (Table 2). The model time step is 1 hour. The CRAY-2 has a peak speed of 1.8 billion floating-point operations-per-second (FLOPS). The version of the OGCM described herein has an averaged speed of 90 million FLOPS on the 4-processor CRAY-2 at Ames. It takes about 6 hours on a CRAY-2 to run one model year.

3 Comparison of model simulations on CRAY-2 and CYBER-205

In the numerical experiment to validate the transfer of the model code from GFDL's CYBER-205 to Ames's CRAY-2, the Richardson number dependent parameterization is used. The initial condition for the experiment consists of climatological-mean January distributions of temperature and salinity (Levitus, 1982) with no currents. Climatological-mean monthly surface wind stress and air temperature are used to force the model for 3 years. The surface wind stress is that of Hellerman and Rosenstein (1983) and the air temperature is that of objective analyses of the Comprehensive Ocean-Atmosphere Data Set (Oort *et al.*, 1987). The model updates its surface boundary conditions at every time step, which are obtained by linear interpolation from the two adjacent monthly means. Snapshots in the middle of each month are used in the analyses presented in this section, and 3-day averaged values are used in the next section.

The version of the GFDL OGCM on CYBER-205 used half precision of 64-bit, i.e., 32-bit, mantissa arithmetic, which reduced the size of model code by nearly 50% so that it was well suited for the 2 million word central memory of the CYBER-205. Because of the 256 million word central memory of a CRAY-2 supercomputer, the size of the OGCM code is of secondary concern so that the full precision of 64-bit mantissa arithmetic is now used. In the process of transferring the OGCM code from CYBER-205 to CRAY-2, we performed two 3-year model integrations to test the effect of different precision on the simulation of the tropical Pacific.

The OGCM code used at Ames is identical to that used at GFDL by Philander *et al.* (1987). The two integrations start from the same initial conditions and are forced with the same atmospheric conditions. The differences between the two integrations are compared at

the end of month 1, month 13, and month 33 along several selected longitudes (150°E , 180° , 150°W , 110°W) and latitudes (10°S , EQ, 10°N). Because the same model is used on the CRAY-2 and CYBER-205, the differences are due to the accumulation of round-off errors introduced by lower precision at every time step.

The comparison of model simulations on CRAY-2 (represented in the diagrams as A) and CYBER-205 (represented as B) at the end of month 1 is shown in Fig. 3 (a), (b) and Fig. 4 (a), (b) for temperature and zonal current, respectively. Temperature distributions are identical and a slight difference is noted in the zonal current distributions.

The differences between the two simulations are more apparent in month 13, as shown in Fig. 5 (a), (b) and Fig. 6 (a), (b). The maximum difference in temperature is located in the eastern equatorial Pacific. Differences between the two simulations are larger for zonal current than for temperature, with maximum deviation of zonal current occurring at 0° to 5°N along 150°W .

In month 33, as shown in Fig. 7 (a) and (b), the maximum difference in temperature is between 4°S and 4°N along 150°W . Differences for the zonal current between the two simulations are strongest between 3°S to 2°N along 150°W and 110°W (Fig. 8 (a) and (b)).

The maximum differences of the mean temperature and zonal current along a section computed from the two simulations was 0.2°C and 5 cm s^{-1} (Tables 3 and 4). Major discrepancies occurred in the eastern equatorial Pacific where there is a strong current shear between the South Equatorial Current and North Equatorial Countercurrent. The agreement between the two simulations was better for month 33 than month 13 along the latitudinal sections and also along longitudinal sections of 150°E and 180° , but the agreement was worse for month 33 than month 13 along longitudinal sections of 150°W and 110°W (Tables 3 and 4). The average (among seven selected sections) root mean square (rms) difference between the temperature signatures was 35% smaller for month 33 than for month 13 (Tables 3 and 4). The average rms differences between the zonal current signatures for month 13 and month 33 were equal to within 5% (Tables 3 and 4).

The CRAY-2 simulation has less variability with small spatial scales than the CYBER-205 result, although the same model with the same initial and boundary conditions is used. The smoother simulated distributions of temperature (Fig. 9) and zonal current (Fig. 10) produced by the CRAY-2 compared to the CYBER-205 are caused by the smaller amount of computational noise associated with the higher precision of the CRAY-2. Computational noise may influence climate predictions (Williamson and Washington, 1973).

4 Climatological seasonal cycle

Seasonally, the trade winds along the equator are intense during the northern autumn when the Intertropical Convergence Zone (ITCZ) is farthest north, and are weak in northern spring when the ITCZ is close to the equator. The westward flowing South Equatorial Current

along the equator is strong when the trade wind is intense, and it is weaker when the strength of the trade wind is also weaker (Fig. 11). During the northern autumn and winter, instability waves with oscillation period of 20 to 30 days occur between 0° and 10°N . Signatures of these instability waves are seen in the temperature and current fields.

The simulated climatological seasonal cycle carried out on the CRAY-2 is similar to the CYBER-205 simulation made by Philander *et al.* (1987). The seasonal cycle of the Equatorial Undercurrent is well simulated, as shown in Fig. 12. Similar to observations (Halpern and Weisberg, 1989), the Equatorial Undercurrent core is located at about 100 m; its speed is strongest (1.2 m s^{-1}) in spring and weakest (0.8 m s^{-1}) in autumn.

5 Discussion

A general circulation model of the tropical Pacific Ocean is described. Two 3-year model integrations from identical initial conditions but performed on two computers, the CRAY-2 at NASA Ames Research Center and the CYBER-205 at GFDL, are compared. The model simulations are very similar to each other, as expected, but the simulation performed with the higher-precision CRAY-2 is smoother than that with the lower-precision CYBER-205. This difference is attributed to the different precision used on the two computing machines. The CYBER-205 uses 32-bit mantissa arithmetic and the CRAY-2 uses 64-bit mantissa arithmetic. Because of different precision used in the simulations, the round-off errors are accumulated at every time step. Comparison of snapshots, on 17th of May and 15th of October during the third year simulation, indicates that the differences appeared primarily with small spatial scales (Figs. 8 and 9). It appears, therefore, that a significant part of variability with small spatial scales simulated by the CYBER-205 is artificially due to truncation errors introduced by the lower precision. This computational error may influence climate predictions as detected by Williamson and Washington (1973).

The model described in this report provides a powerful tool for the study of tropical oceans, such as the dynamics of the North Equatorial Countercurrent and Equatorial Undercurrent. The satellite data assimilation using this model is currently under way.

At the time of this writing, a new version of the GFDL OGCM (Pacanowski *et al.*, 1991) has been released. This new model includes essentially the same dynamics described in section 2.1. In addition, it includes the three subgrid-scale parameterizations described in section 2.2. These different subgrid-scale parameterizations are designed in a modular form so that they can be easily applied to various oceanic problems over a wide range of space and time scales. The new model code also has a multi-tasking capability which allows about 80% parallelism on a four processor CRAY Y-MP. This new version GFDL OGCM will be transferred to CRAY-2 at NASA Ames Research Center in the near future.

References

- Arakawa, A. (1966) Computational design for long-term numerical integration of the equations of fluid motion: two dimensional incompressible flow. Part 1. *Journal of Computational Physics*, 1, 119-143.
- Bryan, K. (1969) A numerical method for the study of the world ocean. *Journal of Computational Physics*, 4, 347-376.
- Bryan, K., and M. D. Cox (1972) An approximate equation of state for numerical models of ocean circulation. *Journal of Physical Oceanography*, 2, 510-514.
- Carton, J. A., and E.C. Hackert (1989) Application of multi-variate statistical objective analysis to the circulation in the tropical Atlantic. *Dynamics of Atmospheres and Oceans*, 13, 491-515.
- Cox, M. D. (1984) A primitive, 3-dimensional model of the ocean. GFDL Ocean Group Technical Report No.1, Geophysical Fluid Dynamics Laboratory, Princeton University, Princeton, New Jersey, 143 pp.
- Derber, J., and A. Rosati (1989) A global oceanic data assimilation system. *Journal of Physical Oceanography*, 19, 1333-1347.
- Ghil, M., and P. Malanotte-Rizzoli (1991) Data assimilation in meteorology and oceanography. *Advances in Geophysics* (submitted).
- Halpern, D. (1980) Variability of near-surface currents in the Atlantic North Equatorial Countercurrent during GATE. *Journal of Physical Oceanography*, 10, 1213-1220.
- Halpern, D. (1987) Observations of annual and El Niño flow variations at 0°, 110°W and 0°, 95°W during 1980-1985. *Journal of Geophysical Research*, 92, 8197-8212.
- Halpern, D., and R. Weisberg (1989) Upper ocean thermal and flow fields at 0°, 28°W (Atlantic) and 0°, 140°W (Pacific) during 1983-1985. *Deep-Sea Research*, 36, 407-418.
- Hellerman, S., and M. Rosenstein (1983) Normal monthly wind stress over the world ocean with error estimates. *Journal of Physical Oceanography*, 13, 1093-1104.
- Leetmaa, A., and M. Ji (1989) Operational hindcasting of the tropical Pacific. *Dynamics of Atmospheres and Oceans*, 13, 465-490.
- Levitus, S. (1982) Climatological atlas of the world ocean. NOAA Professional Paper No. 13, U.S. Government Printing Office, Washington, 173 pp, 17 fiche.
- Mellor, G. L., and T. Yamada (1973) A hierarchy of turbulence closure models for planetary boundary layers. *Journal of the Atmospheric Sciences*, 31, 1791-1806.
- Mellor, G. L., and T. Yamada (1982) Development of a turbulence closure model for geophysical fluid problems. *Review of Geophysics and Space Physics*, 20, 851-875.
- Morlière, A. P., G. Reverdin and J. Merle (1989) Assimilation of temperature profiles in a general circulation model of the tropical Atlantic. *Journal of Physical Oceanography*, 19, 1892-1899.

- Oort, A. H., Y. H. Pan, R. W. Reynolds and C. F. Ropelewski (1987) Historical trends in the surface temperature over the oceans based on the COADS. *Climate Dynamics*, 2, 29-38.
- Pacanowski, R., and S. G. H. Philander (1981) Parameterization of vertical mixing in numerical models of tropical oceans. *Journal of Physical Oceanography*, 11, 1443-1451.
- Pacanowski, R., K. Dixon and A. Rosati (1991) User's Guide to GFDL Modular Ocean Model. Geophysical Fluid Dynamics Laboratory, Princeton University, Princeton, New Jersey, in press.
- Philander, S. G. H., and R. Pacanowski (1980) The generation of equatorial currents. *Journal of Geophysical Research*, 85, 1123-1136.
- Philander, S. G. H., and A. D. Seigel (1985) Simulation of El Niño of 1982-83. In "*Coupled Ocean-Atmosphere Models*" edited by J.C.J. Nihoul, Elsevier, 517-541.
- Philander, S. G. H., W. J. Hurlin and A. D. Seigel (1987) A model of the seasonal cycle in the tropical Pacific Ocean. *Journal of Physical Oceanography*, 17, 1986-2002.
- Philander, S. G. H., R. C. Pacanowski, N. C. Lau and M. J. Nath (1990) A simulation of the Southern Oscillation. Part 2: Results from high-resolution coupled General Circulation Models of the ocean and atmosphere. *Journal of Climate*, in press.
- Rosati, A., and K. Miyakoda (1988) A general circulation model for upper ocean simulation. *Journal of Physical Oceanography*, 18, 1601-1626.
- Semtner, A. J., and W. R. Holland (1980) Numerical simulation of equatorial ocean circulation. Part 1: A basic case in turbulent equilibrium. *Journal of Physical Oceanography*, 10, 667-693.
- Williamson, D. L., and W. M. Washington (1973) On the importance of precision for short-range forecasting and climate simulation. *Journal of Applied Meteorology*, 12, 1254-1258.

Table 1: Values of Newtonian damping coefficient, ϵ , near the southern and northern boundaries.

j-value	latitude	damping coefficient (second)
1	28.84S	1.98E-6
2	26.53S	2.31E-6
3	24.29S	1.98E-6
4	22.15S	1.16E-6
5	20.15S	3.39E-7
94	32.26N	1.55E-7
95	34.78N	5.79E-7
96	37.41N	1.16E-6
97	40.11N	1.74E-6
98	42.89N	2.16E-6
99	45.71N	2.31E-6
100	48.57N	2.16E-6

Table 2: Vertical levels, grid sizes (m), and corresponding depths of bottom of layer (m).

level	grid size	depth
1	10.0	10.0
2	10.0	20.0
3	10.0	30.0
4	10.0	40.0
5	10.0	50.0
6	10.0	60.0
7	10.0	70.0
8	10.0	80.0
9	10.0	90.0
10	10.0	100.0
11	12.5	112.5
12	15.0	127.5
13	17.5	145.0
14	20.0	165.0
15	25.0	190.0
16	30.0	220.0
17	40.0	260.0
18	57.0	317.0
19	91.0	408.0
20	151.0	559.0
21	242.0	801.0
22	357.0	1158.0
23	475.0	1633.0
24	566.0	2199.0
25	650.0	2849.0
26	650.0	3499.0
27	650.0	4149.0

Table 3: The mean value and root mean square of the difference field between model simulations on CRAY-2 and CYBER-205 along 10°S, EQ, and 10°N.

statistics (UCLA-GFDL)		temperature (degree)		
		month 01	month 13	month 33
10N	mean	0.00	-0.01	0.00
	rms	0.01	0.11	0.01
EQ	mean	0.00	0.05	0.06
	rms	0.02	0.37	0.25
10S	mean	0.00	-0.01	0.01
	rms	0.01	0.11	0.01
average	mean	0.00	0.01	0.02
	rms	0.01	0.23	0.15

statistics (UCLA-GFDL)		zonal current (cm/sec)		
		month 01	month 13	month 33
10N	mean	0.67	-1.19	-0.03
	rms	2.15	4.01	0.53
EQ	mean	0.16	-3.66	-0.30
	rms	3.94	14.12	13.19
10S	mean	-0.63	-1.58	0.00
	rms	1.91	2.22	0.22
average	mean	0.07	-2.14	-0.11
	rms	2.82	8.57	7.62

Table 4: The mean value and root mean square of the difference field between model simulations on CRAY-2 and CYBER-205 along 150°E, 180°, 150°W, and 110°W.

statistics (UCLA-GFDL)		temperature (degree)		
		month 01	month 13	month 33
150E	mean	0.00	-0.01	0.00
	rms	0.00	0.09	0.01
180	mean	0.00	-0.04	-0.04
	rms	0.01	0.06	0.05
150W	mean	-0.01	-0.17	-0.03
	rms	0.02	0.20	0.16
110W	mean	0.00	0.13	0.01
	rms	0.01	0.22	0.11
average	mean	0.00	-0.02	-0.02
	rms	0.01	0.16	0.10

statistics (UCLA-GFDL)		zonal current (cm/sec)		
		month 01	month 13	month 33
150E	mean	-1.08	-0.54	-0.01
	rms	1.22	5.86	0.66
180	mean	-1.24	-2.01	0.06
	rms	4.17	6.61	2.14
150W	mean	-3.76	-3.52	-4.52
	rms	4.06	11.41	16.82
110W	mean	-0.99	-1.38	1.87
	rms	2.18	5.24	7.35
average	mean	-1.77	-1.86	-0.65
	rms	3.17	7.68	9.25

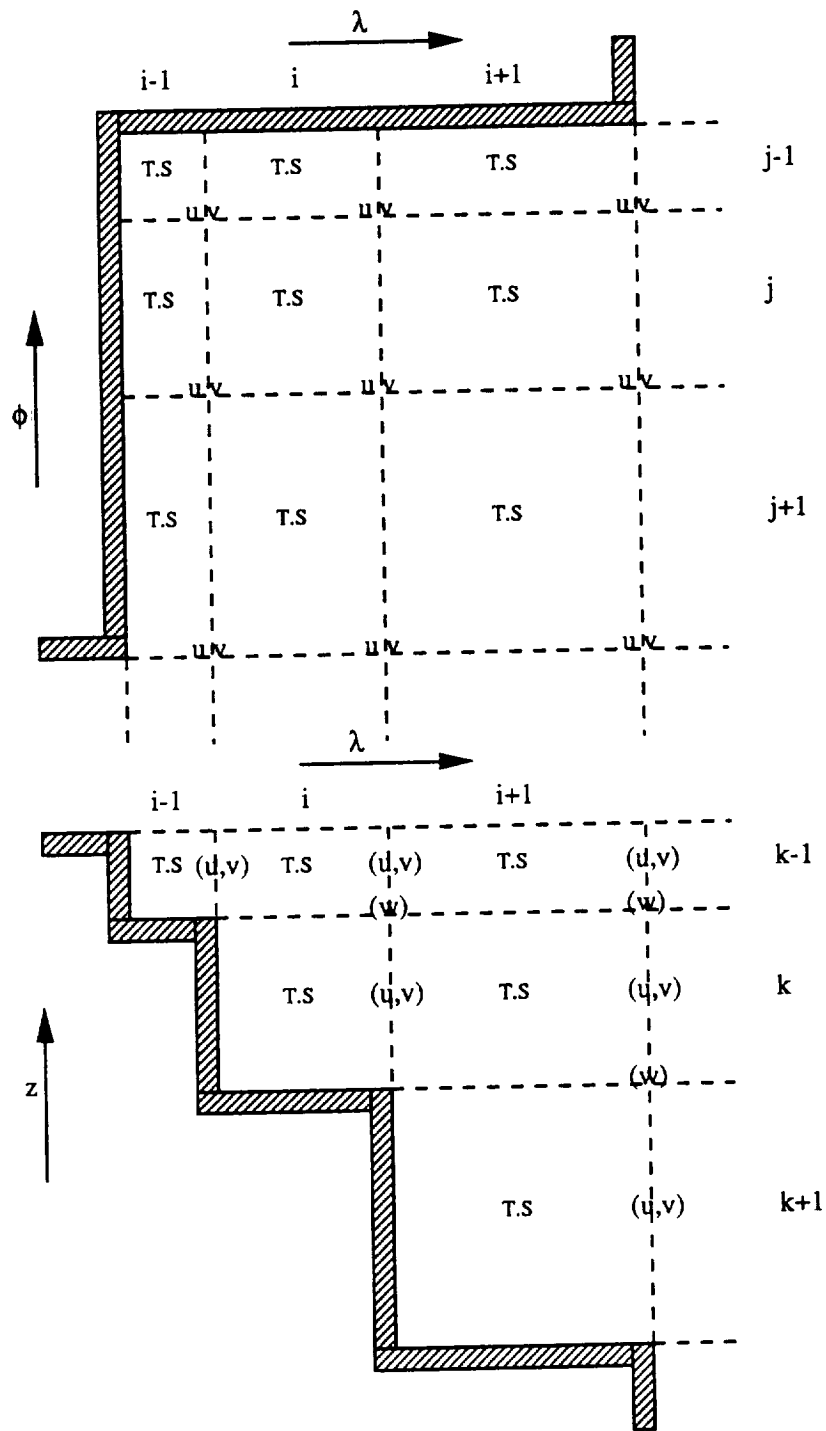


Fig. 1 Configurations of model grids (after Cox, 1984). Temperature, salinity and velocity are given by T, S, u, v and w. The j-value for $0^{\circ}17'N$ is 45. The i-value for 180° is 51.

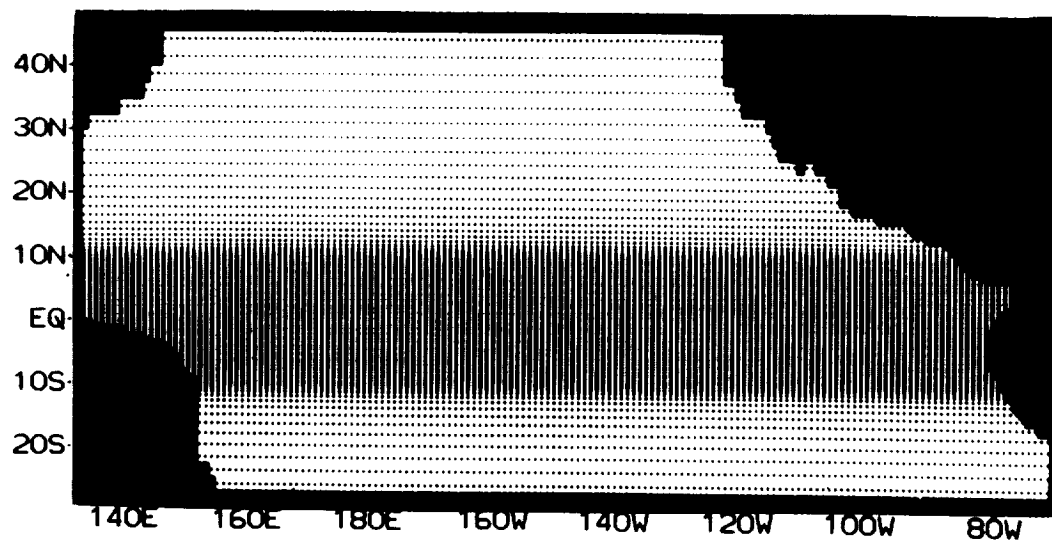


Fig. 2 The model geometry and distributions of model horizontal grids (after Philander *et al.*, 1987).

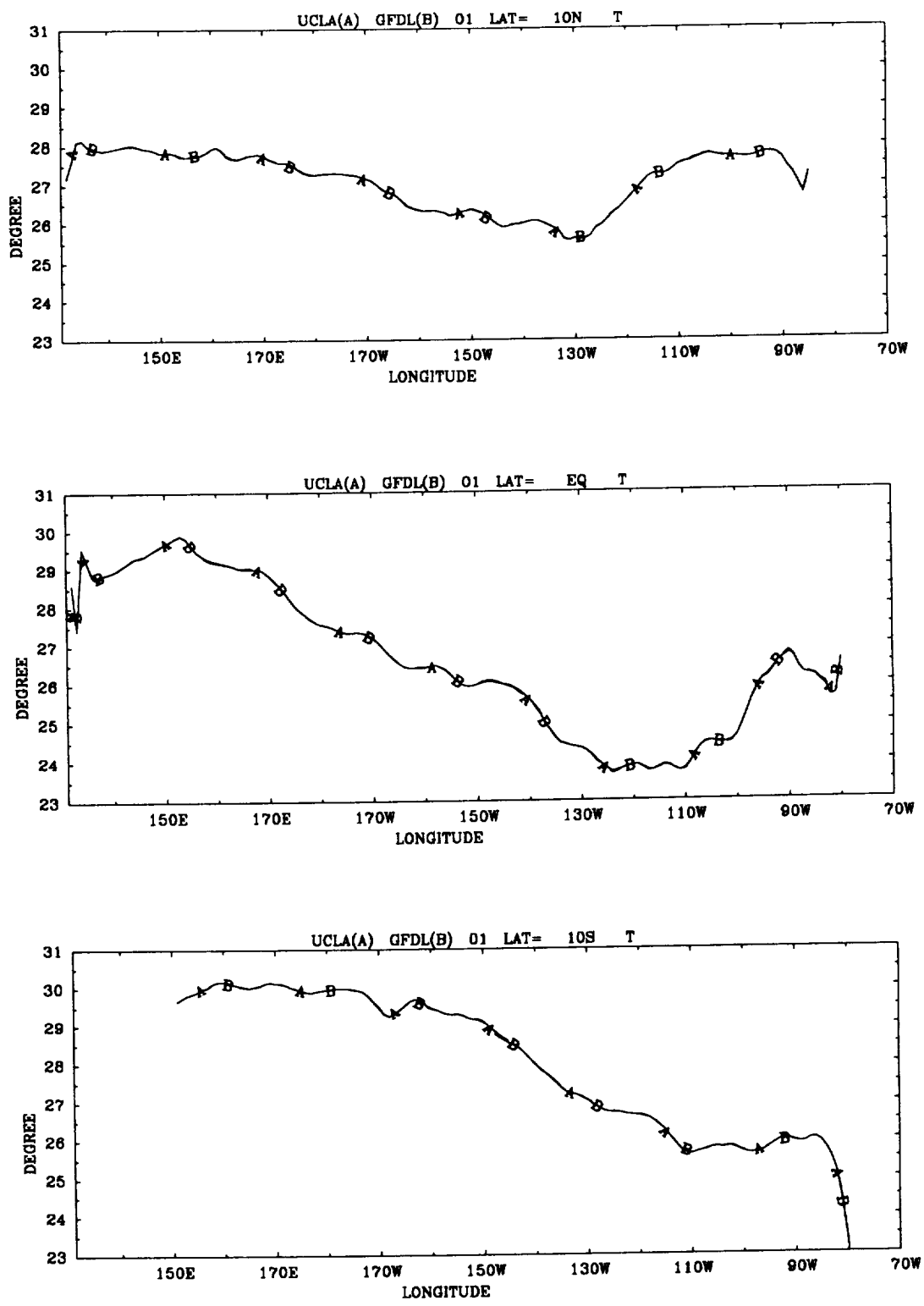


Fig. 3 (a) Surface temperature distributions along 10°S, EQ, and 10°N on 15 February of the first year simulated on CRAY-2 at NASA Ames Research Center (represented as A) and CYBER-205 at GFDL (represented as B).

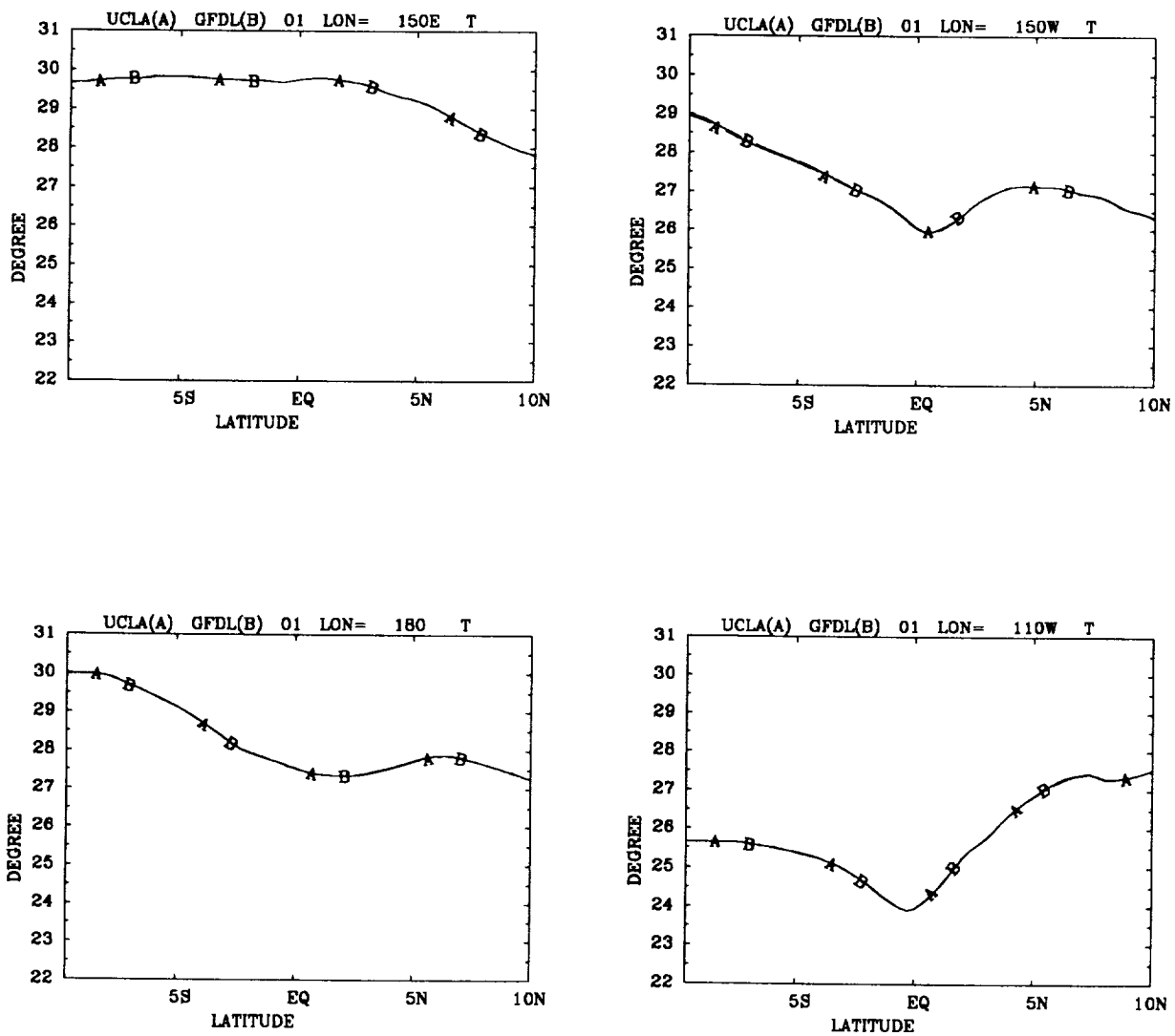


Fig. 3 (b) Surface temperature distributions along 150°E , 180° , 150°W , and 110°W on 15 February of the first year simulated on CRAY-2 at NASA Ames Research Center (represented as A) and CYBER-205 at GFDL (represented as B).

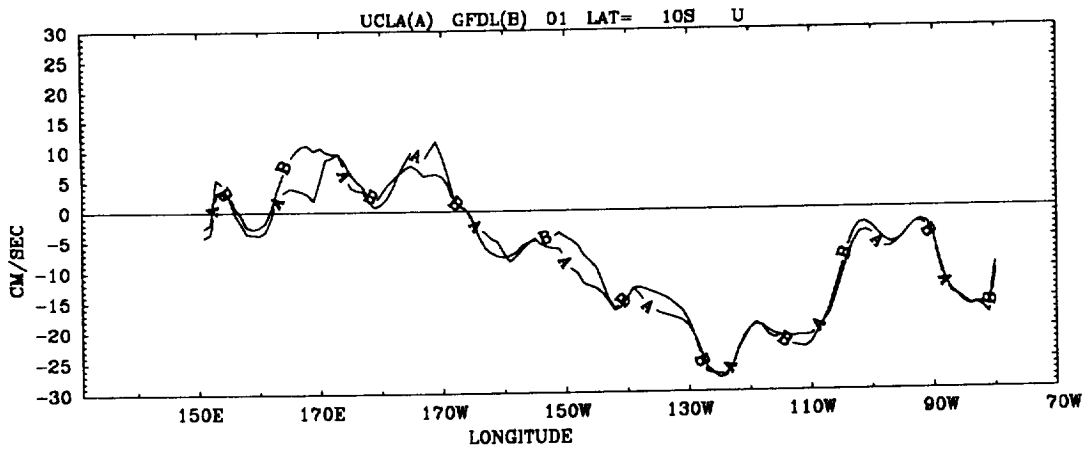
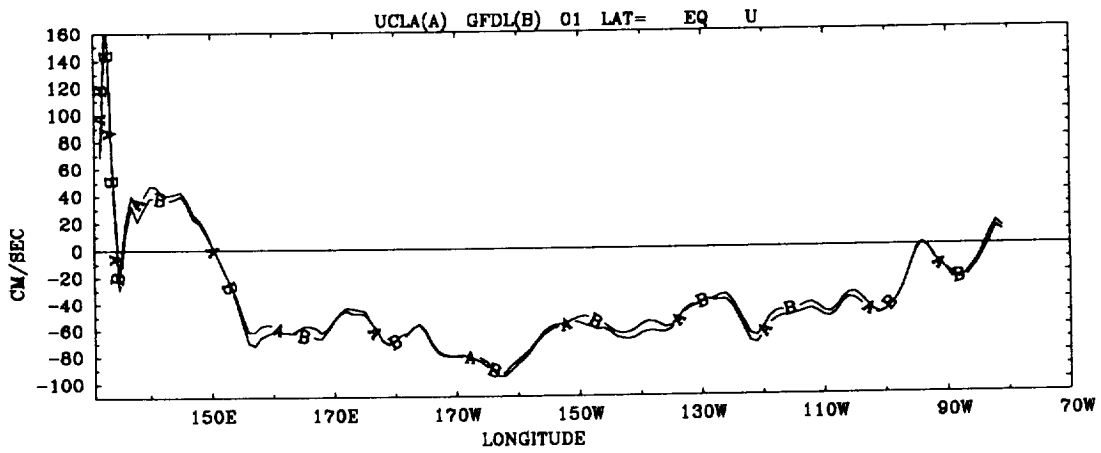
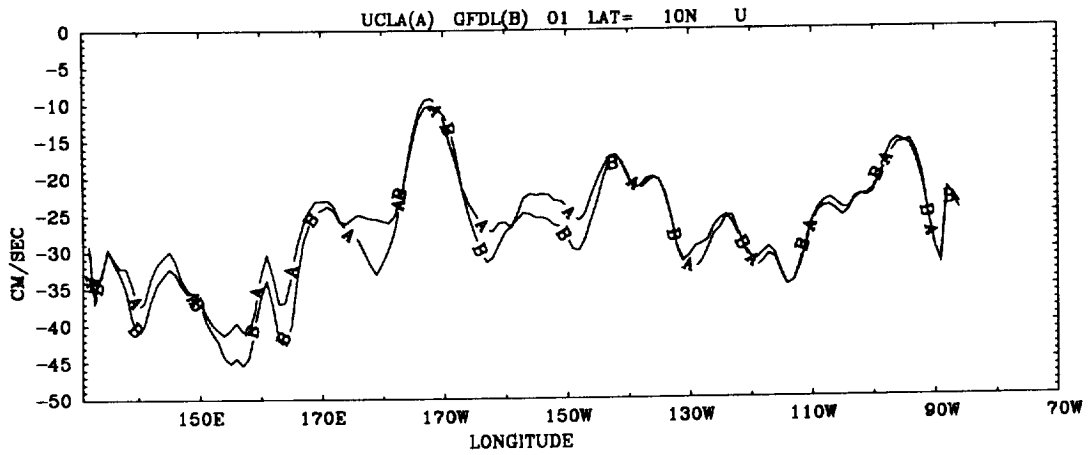


Fig. 4 (a) The same as Fig. 3 (a) but for surface zonal current distributions.

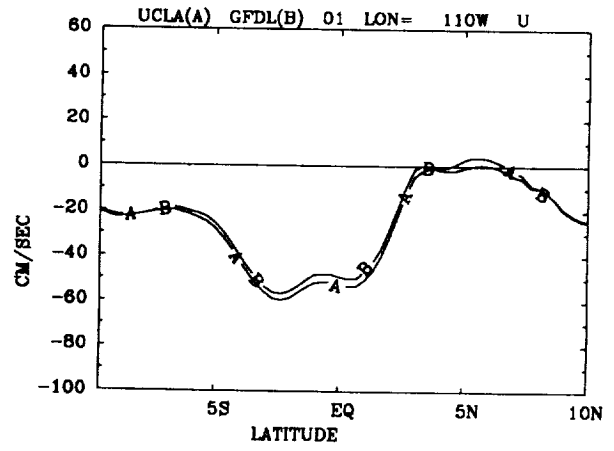
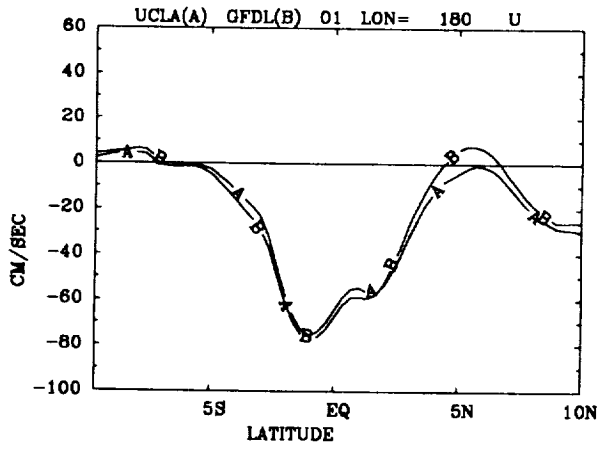
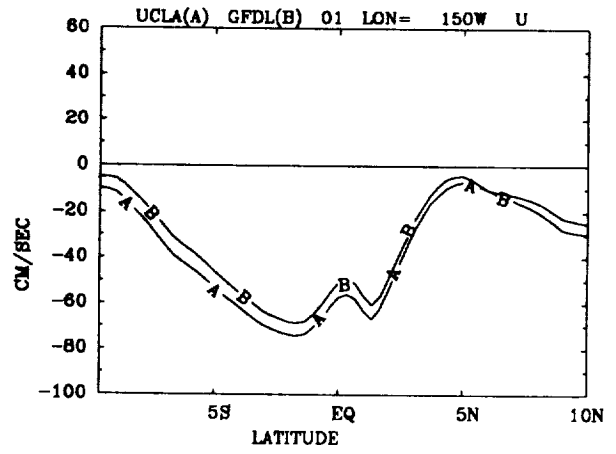
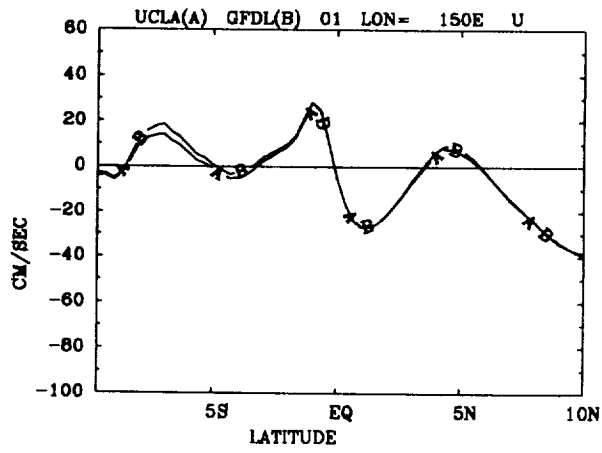


Fig. 4 (b) The same as Fig. 3 (b) but for surface zonal current distributions.

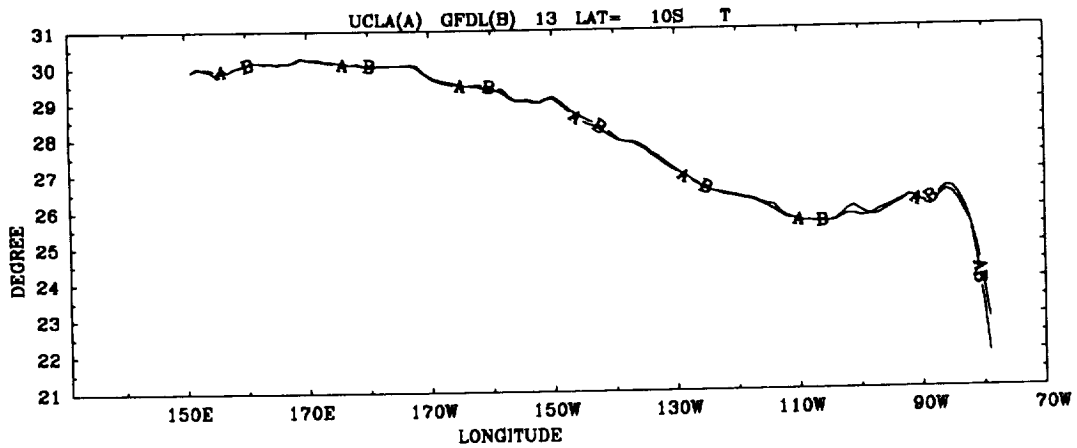
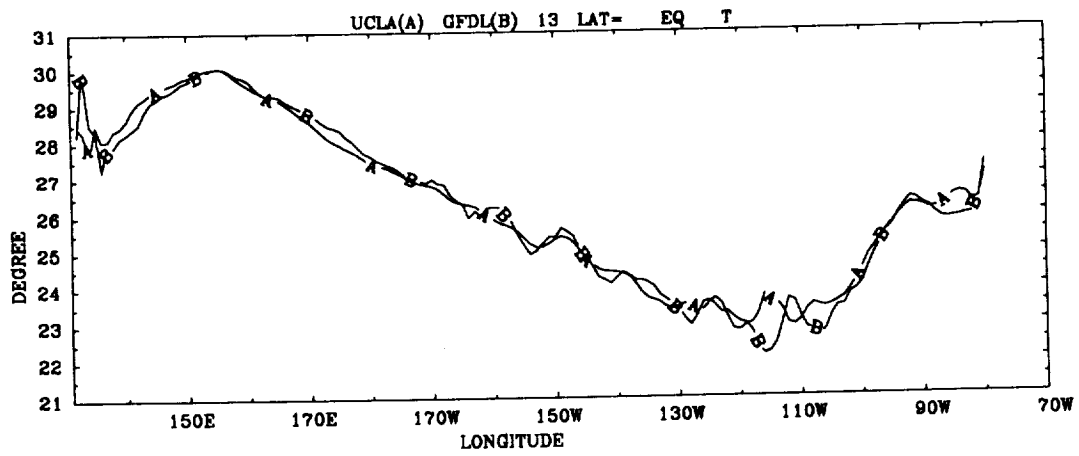
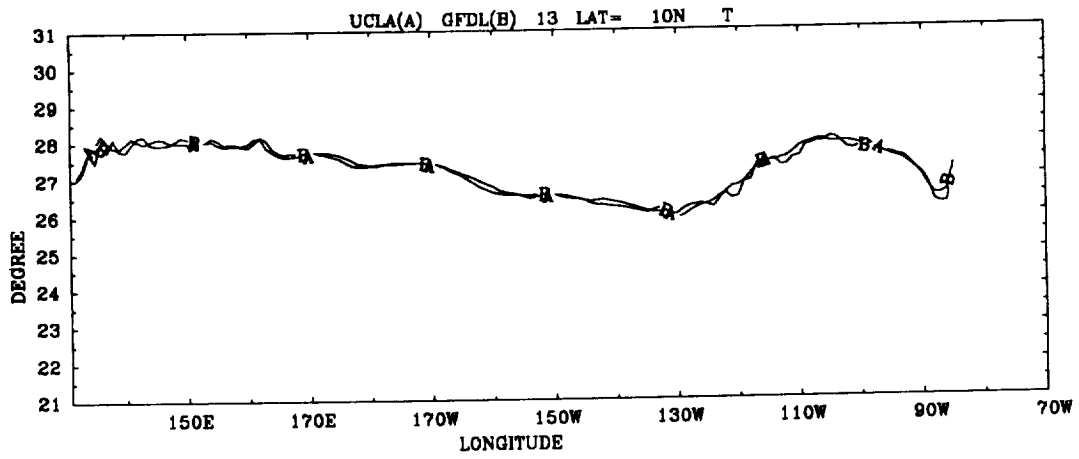


Fig. 5 (a) The same as Fig. 3 (a) but on 15 February during the second year simulation.

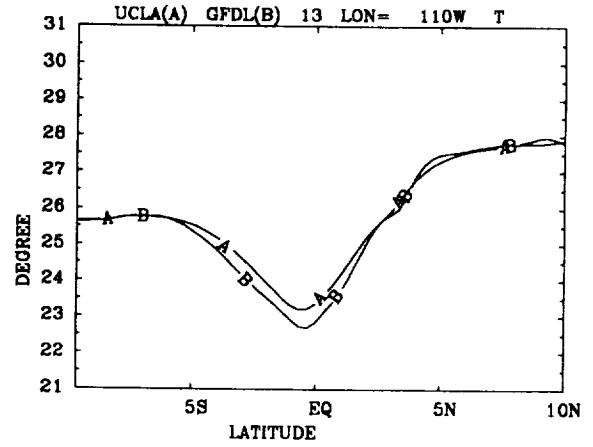
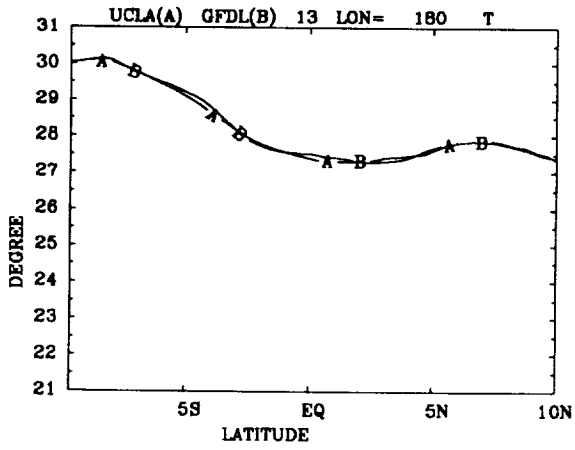
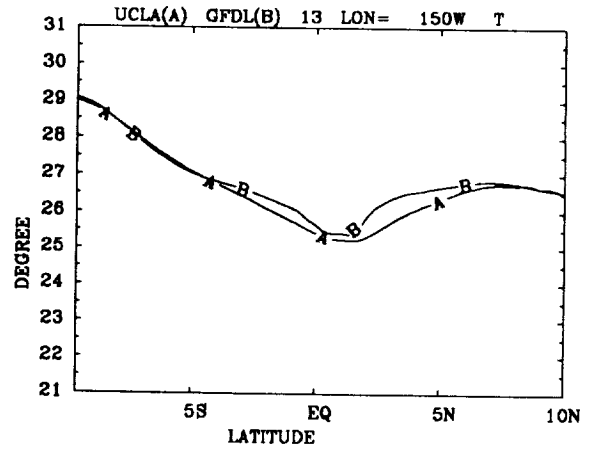
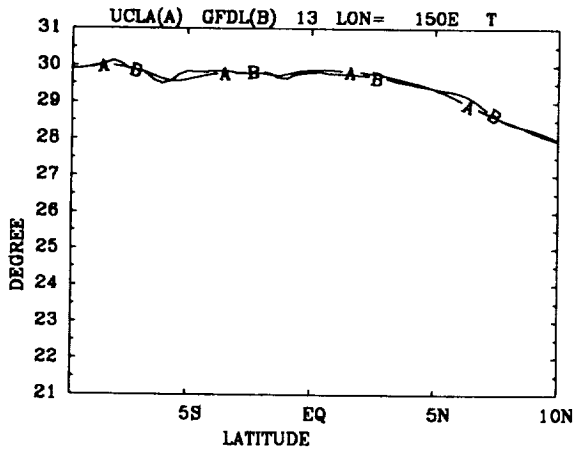


Fig. 5 (b) The same as Fig. 3 (b) but on 15 February during the second year simulation.

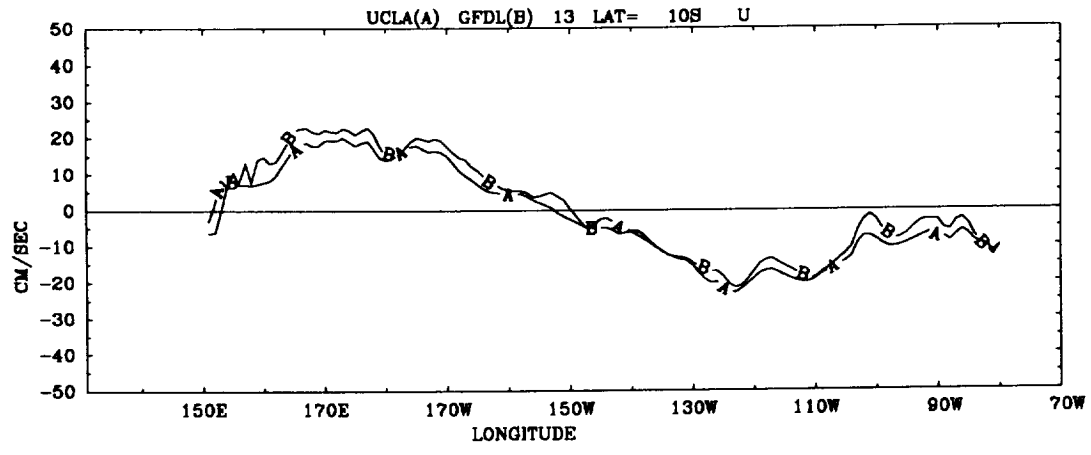
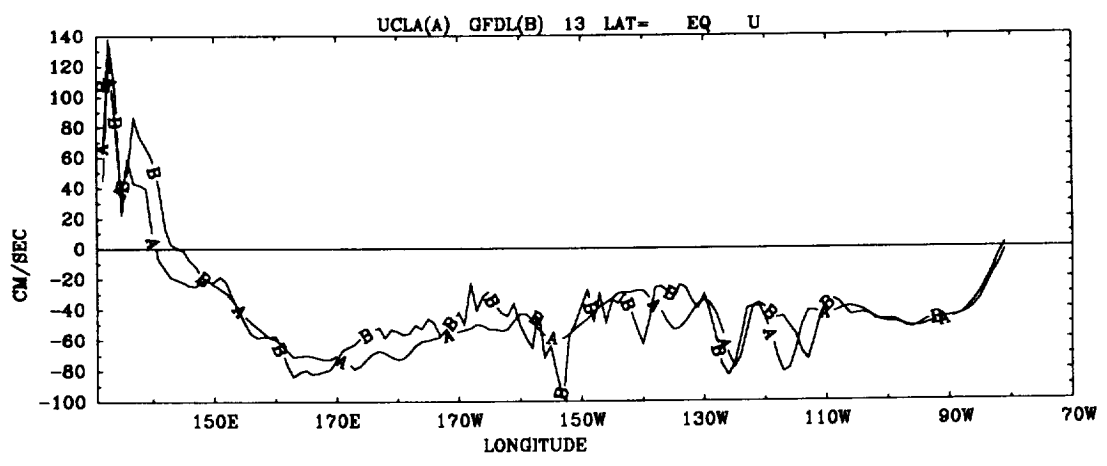
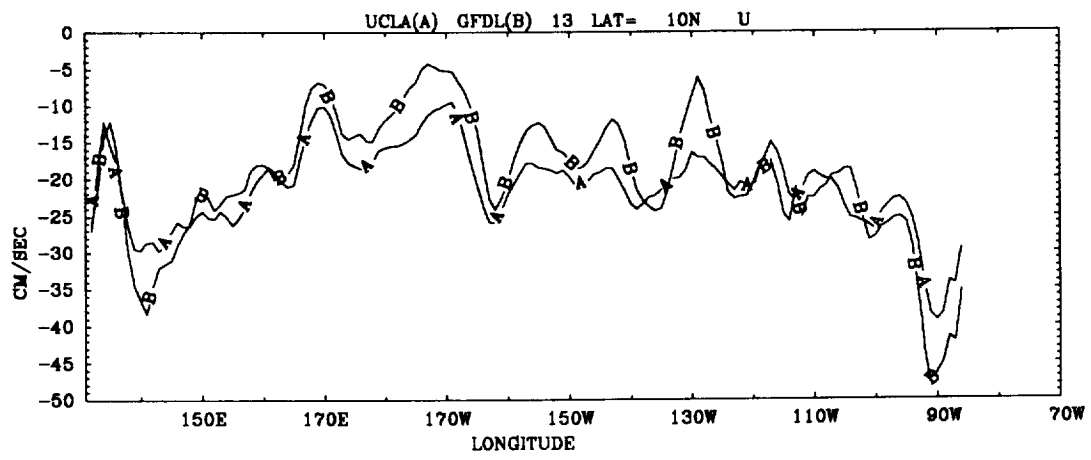


Fig. 6 (a) The same as Fig. 4 (a) but on 15 February during the second year simulation.

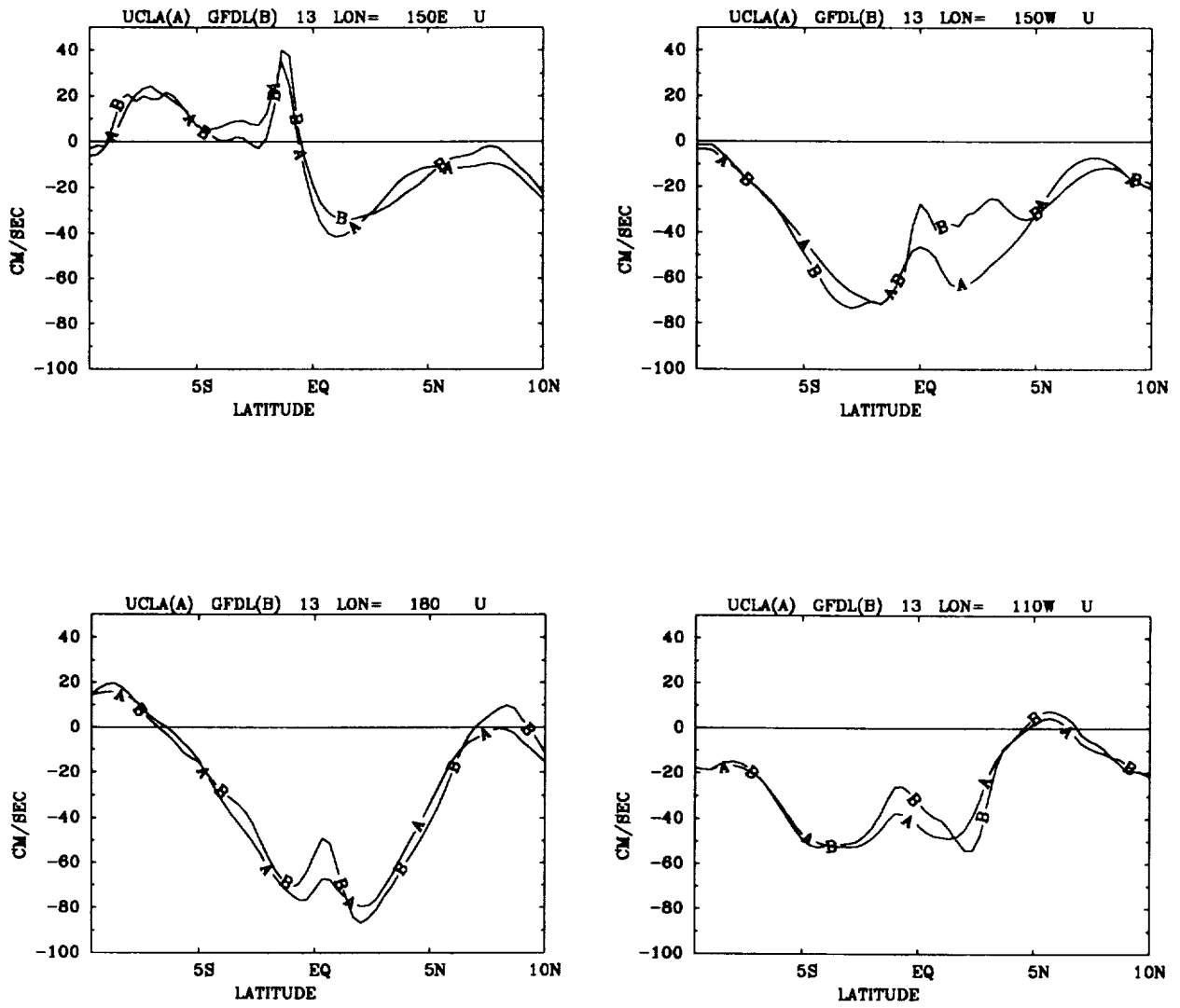


Fig. 6 (b) The same as Fig. 4 (b) but on 15 February during the second year simulation.

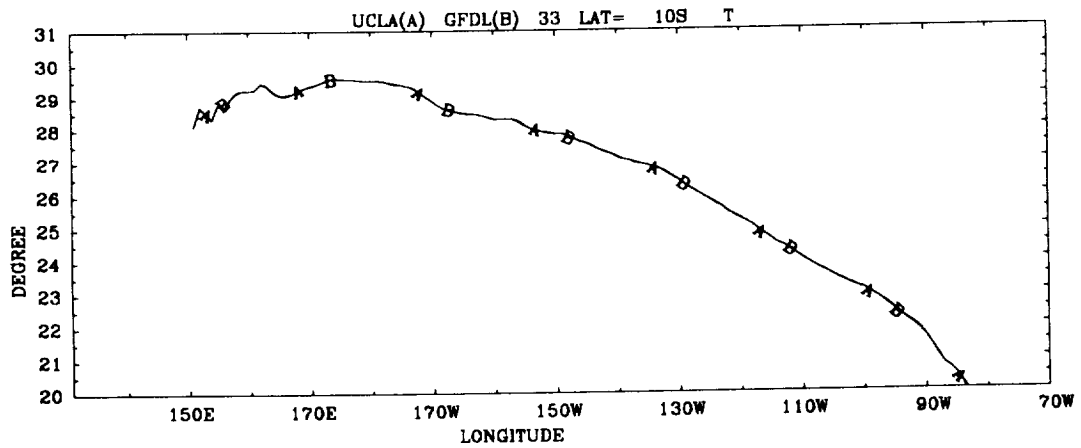
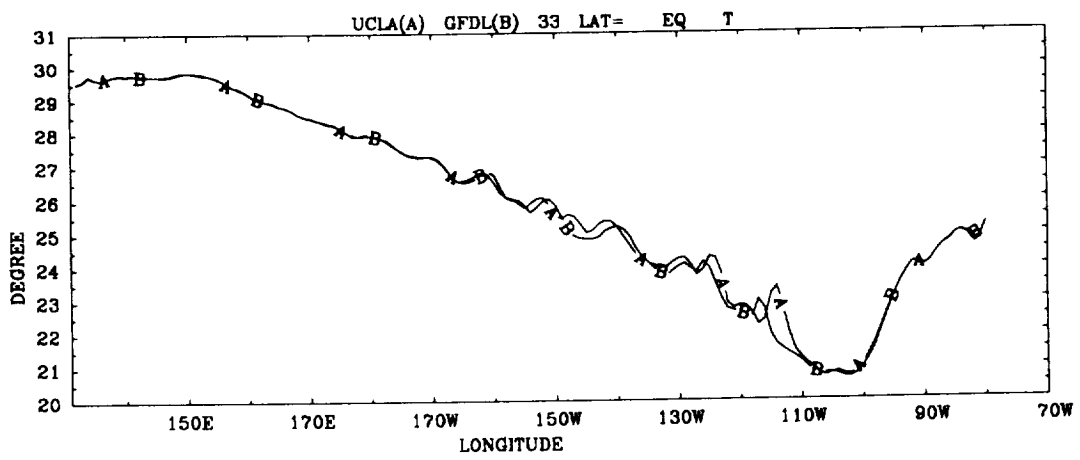
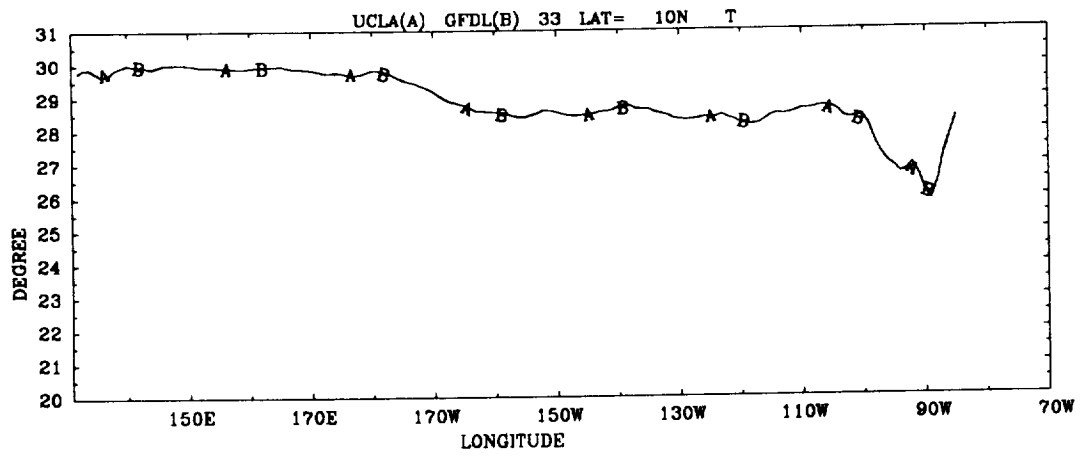


Fig. 7 (a) The same as Fig. 3 (a) but on 15 October during the third year simulation.

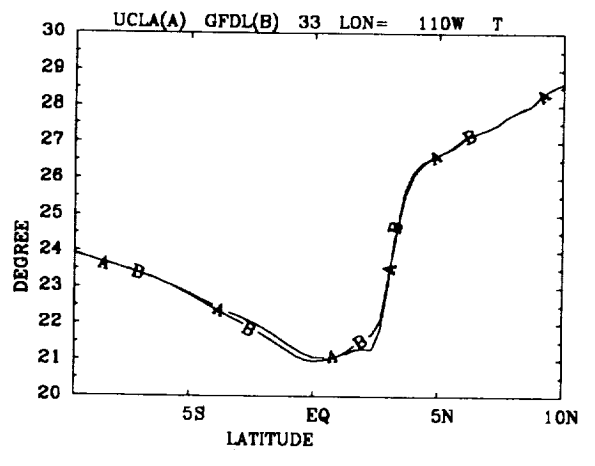
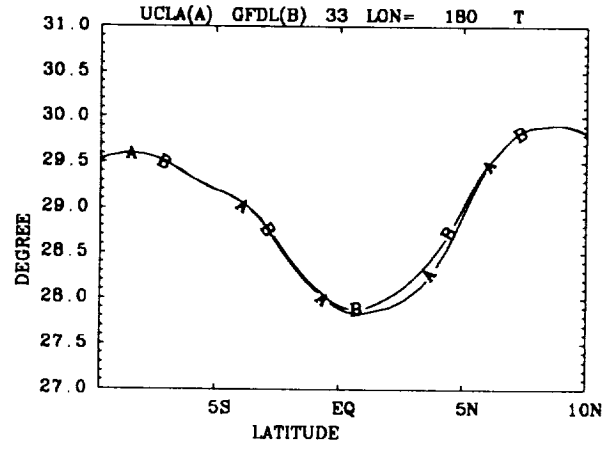
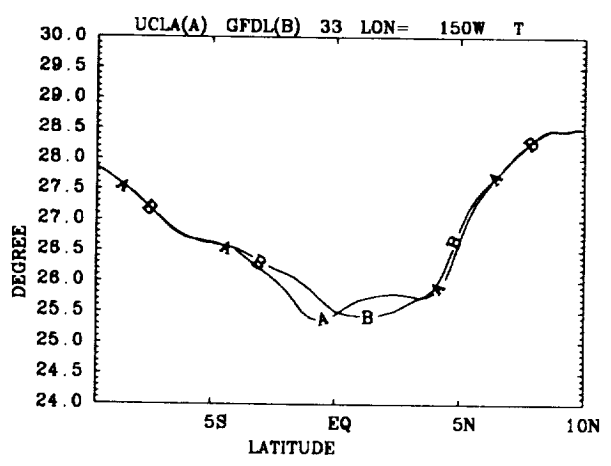
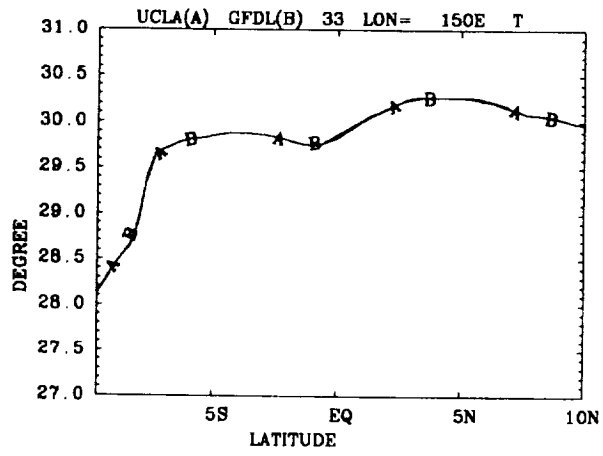


Fig. 7 (b) The same as Fig. 3 (b) but on 15 October during the third year simulation.

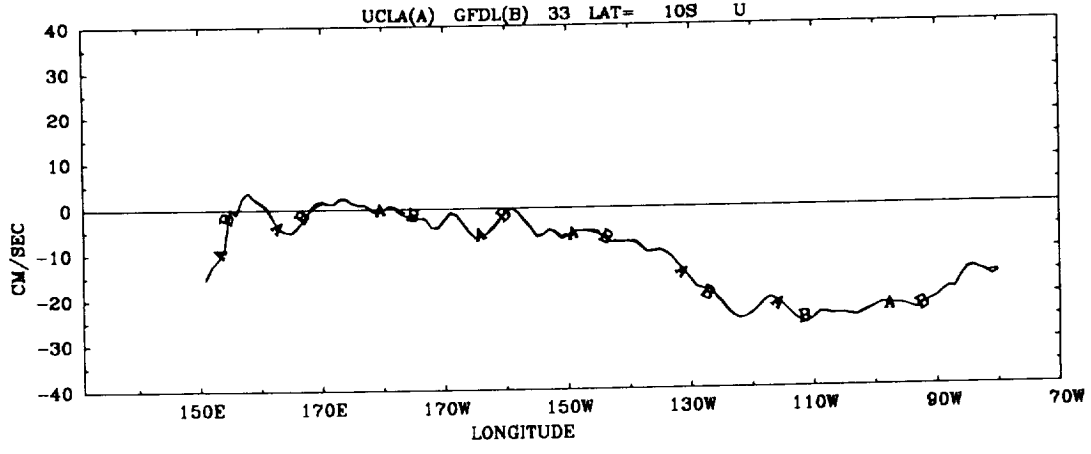
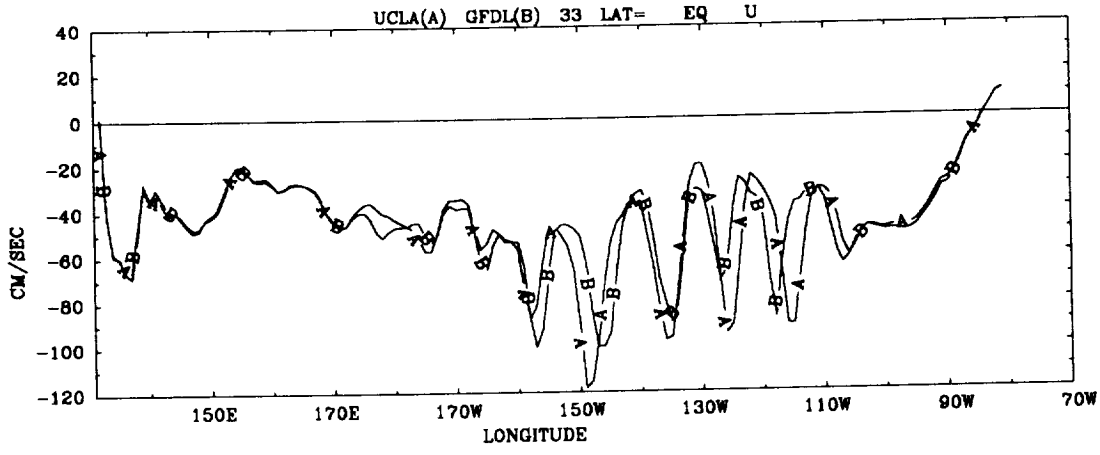
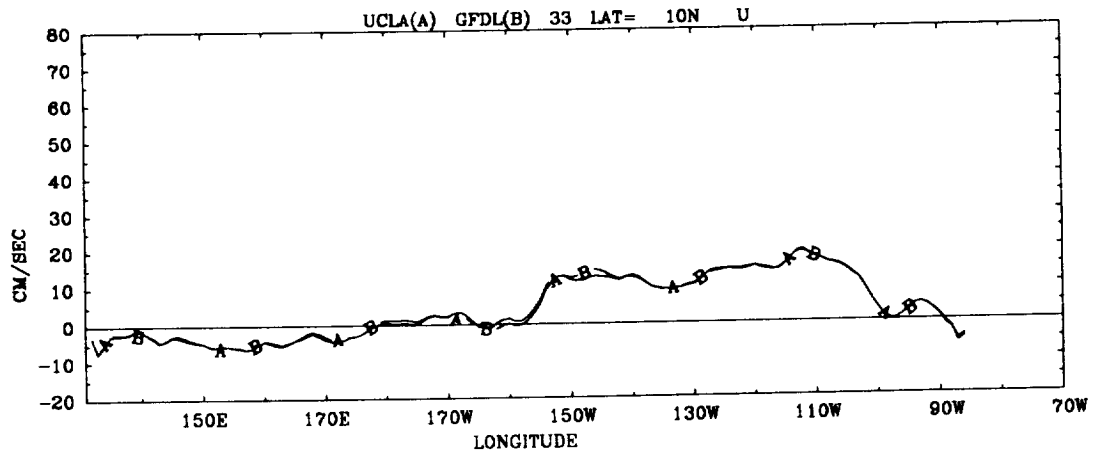


Fig. 8 (a) The same as Fig. 4 (a) but on 15 October during the third year simulation.

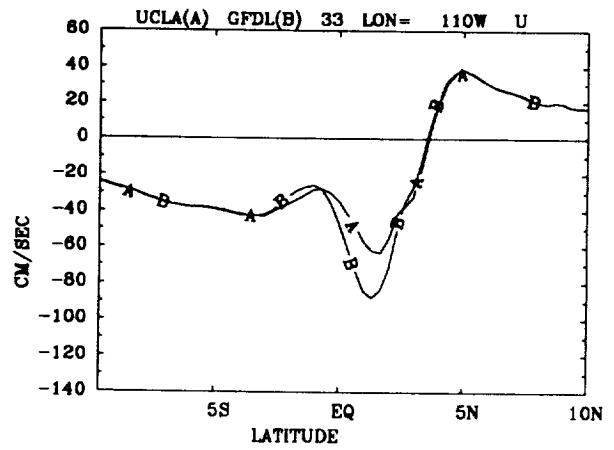
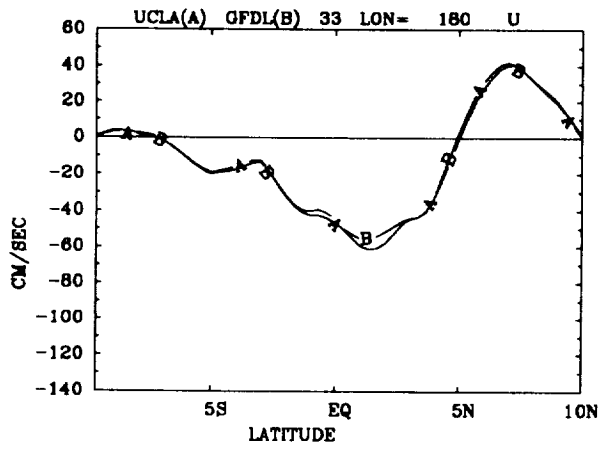
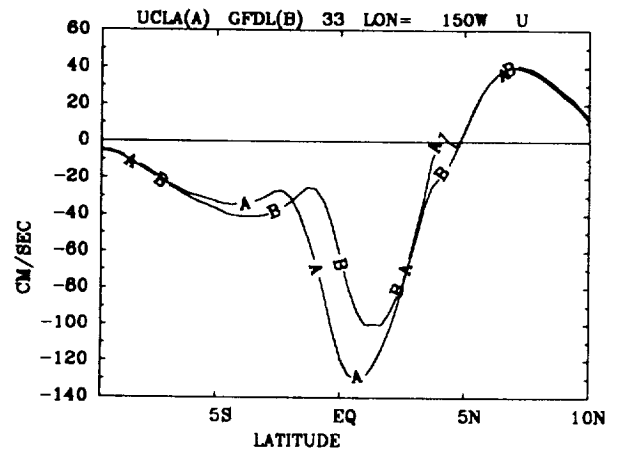
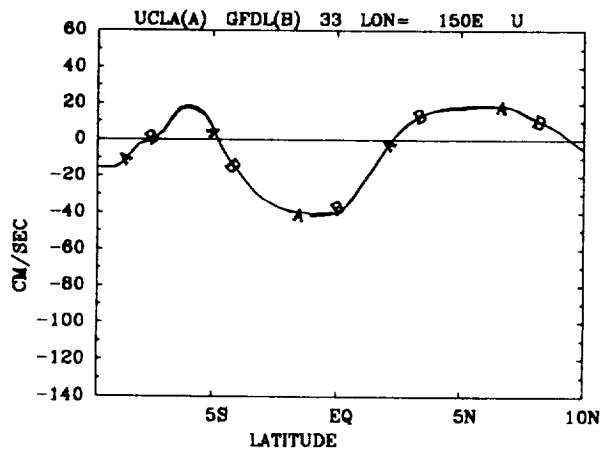


Fig. 8 (b) The same as Fig. 4 (b) but on 15 October during the third year simulation.

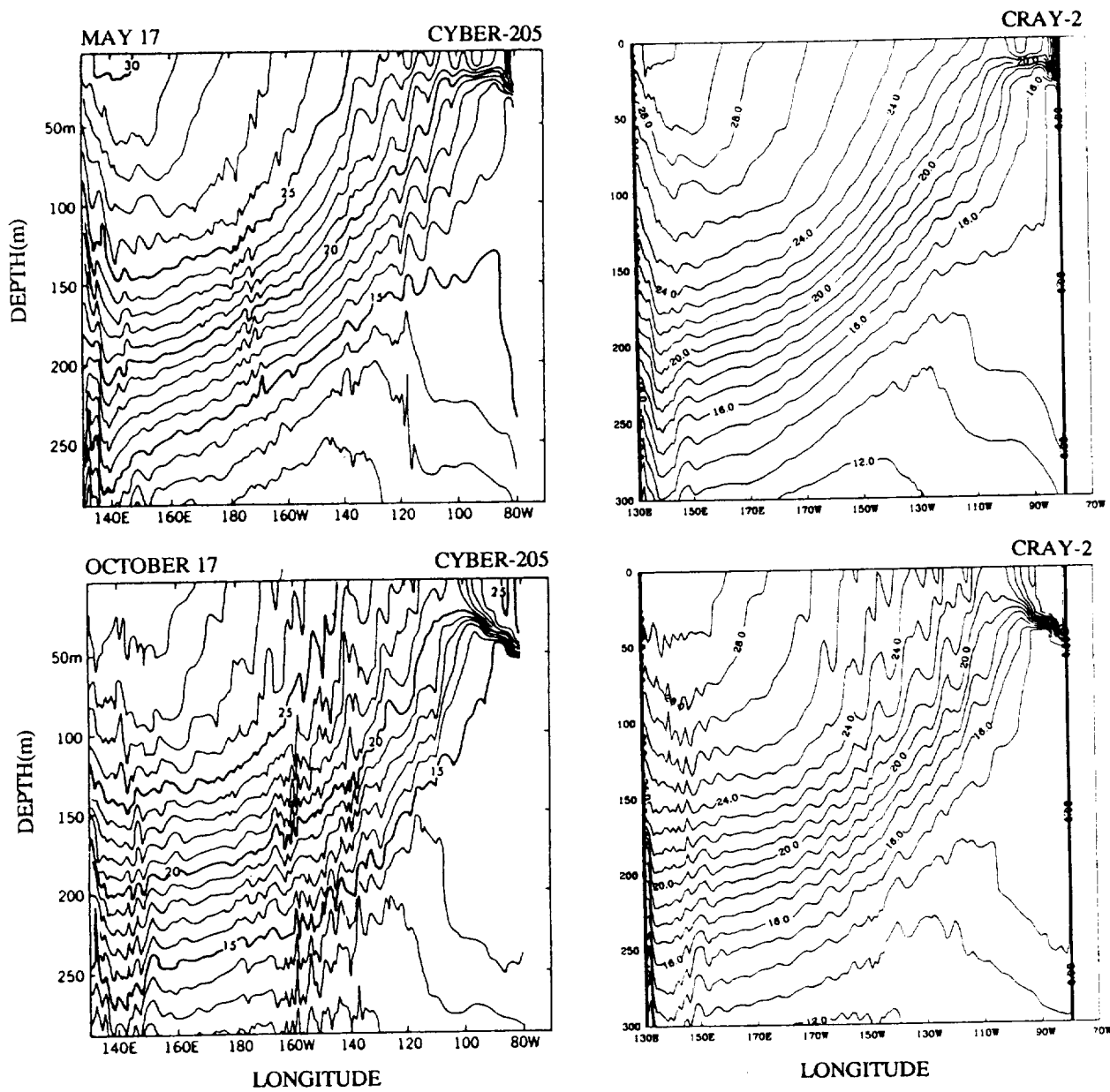


Fig. 9 Temperature ($^{\circ}\text{C}$) sections along the equator on 17 May and 15 October simulated on a CYBER-205 at GFDL (Philander *et al.*, 1987) and a CRAY-2 at NASA Ames Research Center. Note that vertical and horizontal scales are slightly different.

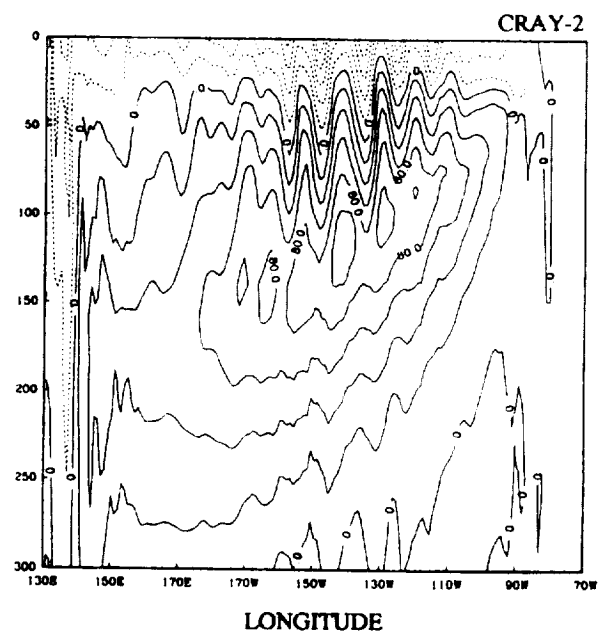
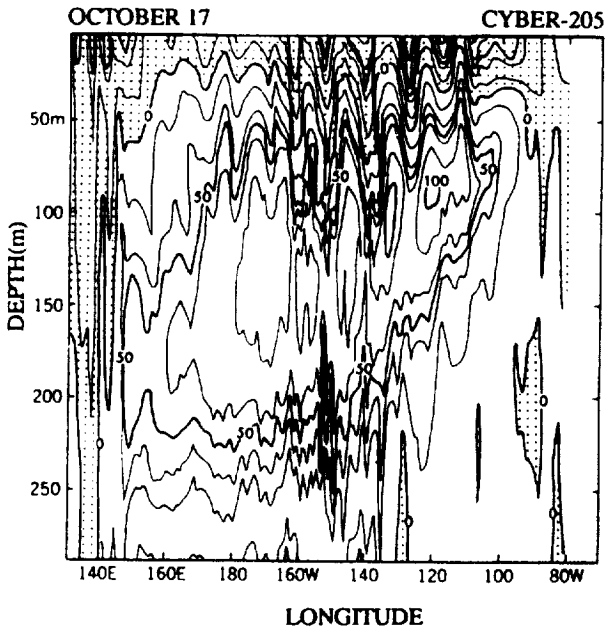
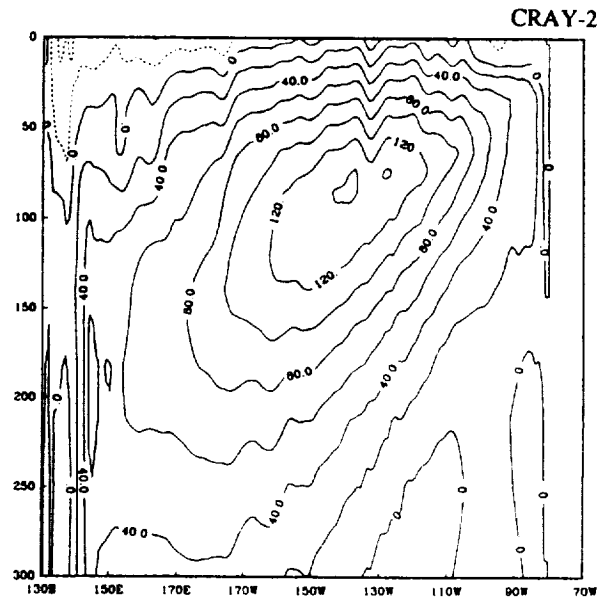
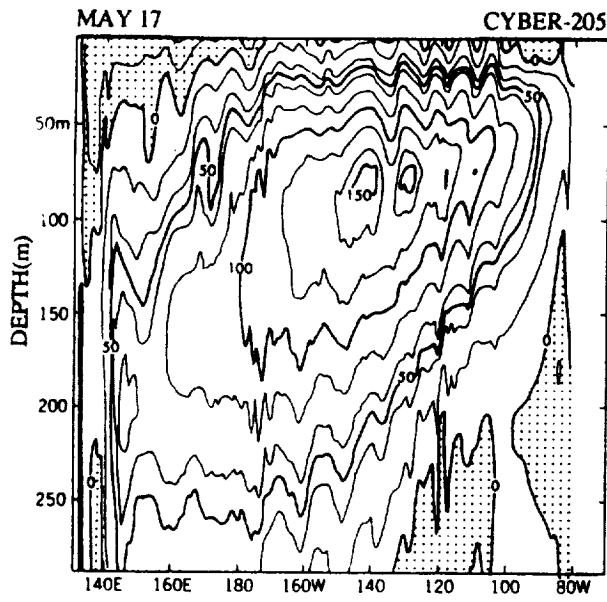


Fig. 10 The same as Fig. 9 but for zonal current (cm s^{-1}).

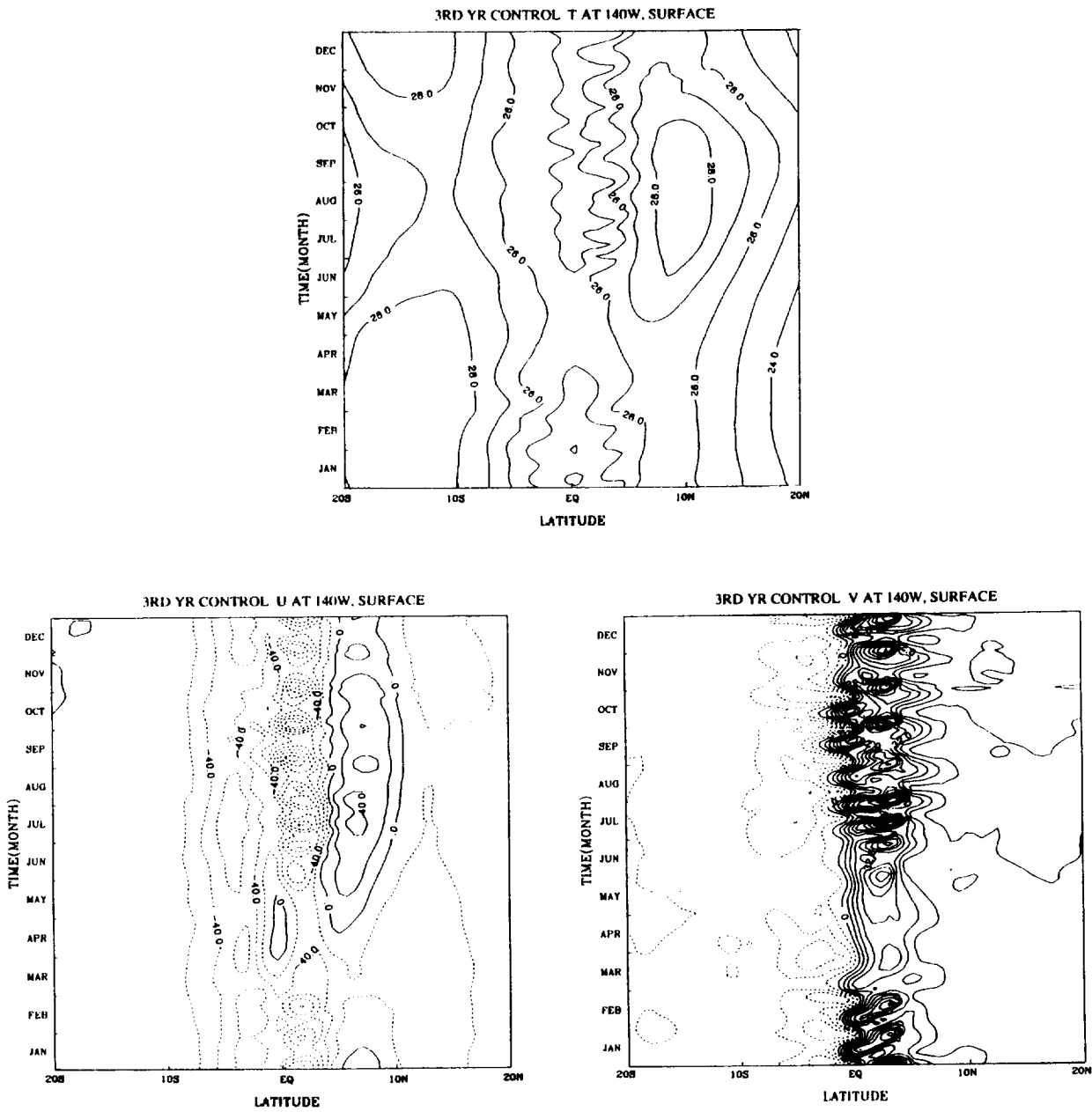


Fig. 11 Seasonal variations of the surface temperature ($^{\circ}\text{C}$), zonal and meridional current (cm s^{-1}) at 140°W . Positive values in current indicate eastward and northward direction.

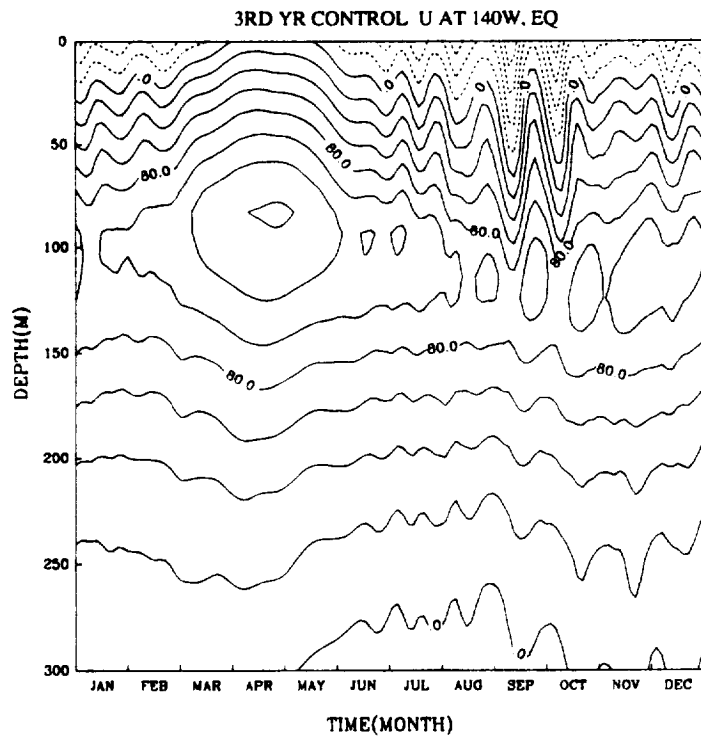
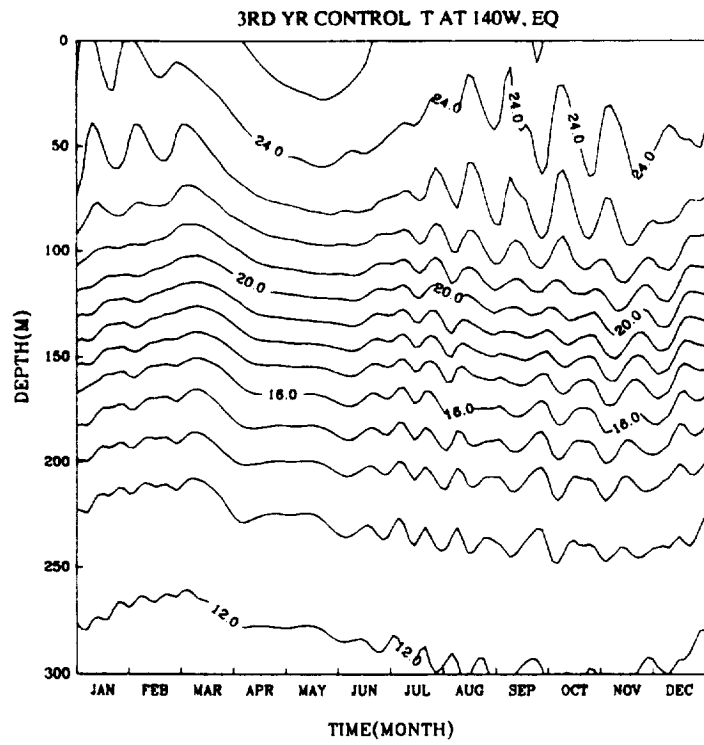


Fig. 12 Seasonal variations of temperature ($^{\circ}\text{C}$) and zonal current (cm s^{-1}) at 140°W , EQ.

TECHNICAL REPORT STANDARD TITLE PAGE

1. Report No. 91-9	2. Government Accession No.	3. Recipient's Catalog No.	
4. Title and Subtitle A Pacific Ocean General Circulation Model for Satellite Data Assimilation		5. Report Date February 1991	
		6. Performing Organization Code	
7. Author(s) Y. Chao, D. Halpern, C.R. Mechoso		8. Performing Organization Report No.	
9. Performing Organization Name and Address JET PROPULSION LABORATORY California Institute of Technology 4800 Oak Grove Drive Pasadena, California 91109		10. Work Unit No.	
		11. Contract or Grant No. NAS7-918	
		13. Type of Report and Period Covered External Report JPL Publication	
12. Sponsoring Agency Name and Address NATIONAL AERONAUTICS AND SPACE ADMINISTRATION Washington, D.C. 20546		14. Sponsoring Agency Code RE4 BP-578-22-26-01-00	
		15. Supplementary Notes	
16. Abstract A tropical Pacific Ocean General Circulation Model (OGCM) to be used in satellite data assimilation studies is described. The transfer of the OGCM from a CYBER-205 at NOAA's Geophysical Fluid Dynamics Laboratory to a CRAY-2 at NASA's Ames Research Center is documented. Two 3-year model integrations from identical initial conditions but performed on those two computers are compared. The model simulations are very similar to each other, as expected, but the simulations performed with the higher-precision CRAY-2 is smoother than that with the lower-precision CYBER-205. The CYBER-205 and CRAY-2 use 32 and 64-bit mantissa arithmetic, respectively. The major features of the oceanic circulation in the tropical Pacific, namely the North Equatorial Current, the North Equatorial Countercurrent, the South Equatorial Current, and the Equatorial Undercurrent, are realistically produced and their seasonal cycles are described. The OGCM provides a powerful tool for study of tropical oceans and for assimilation of satellite altimetry data.			
17. Key Words (Selected by Author(s)) Dynamic Oceanography; Meteorology and Climatology; Physical Oceanography		18. Distribution Statement Unclassified; unlimited	
19. Security Classif. (of this report) Unclassified	20. Security Classif. (of this page) Unclassified	21. No. of Pages	22. Price



—

